Am J Physiol Regul Integr Comp Physiol 309: R235–R246, 2015.
First published June 10, 2015; doi:10.1152/ajpregu.00052.2015.

Differential localization of ion transporters suggests distinct cellular mechanisms for calcification and photosynthesis between two coral species

Katie L. Barott, Sidney O. Perez, Lauren B. Linsmayer, and Martin Tresguerres
Scripps Institution of Oceanography, University of California San Diego, La Jolla, California

Submitted 12 February 2015; accepted in final form 8 June 2015

Barott KL, Perez SO, Linsmayer LB, Tresguerres M. Differential localization of ion transporters suggests distinct cellular mechanisms for calcification and photosynthesis between two coral species. *Am J Physiol Regul Integr Comp Physiol* 309: R235–R246, 2015. First published June 10, 2015; doi:10.1152/ajpregu.00052.2015.—Ion transport is fundamental for multiple physiological processes, including but not limited to pH regulation, calcification, and photosynthesis. Here, we investigated ion-transporting processes in tissues from the corals *Acropora yongei* and *Stylophora pistillata*, representatives of the complex and robust clades that diverged over 250 million years ago. Antibodies against complex IV revealed that mitochondria, an essential source of ATP for energetically costly ion transporters, were abundant throughout the tissues of *A. yongei*. Additionally, transmission electron microscopy revealed septate junctions in all cell layers of *A. yongei*, as previously reported for *S. pistillata*, as well as evidence for transcellular vesicular transport in calicoblastic cells. Antibodies against the alpha subunit of Na^+/K^+-ATPase (NKA) and plasma membrane Ca^{2+}-ATPase (PMCA) immunolabeled cells in the calicoblastic epithelium of both species, suggesting conserved roles in calcification. However, NKA was abundant in the apical membrane of the oral epithelium in *A. yongei* but not *S. pistillata*, while PMCA was abundant in the gastroderm of *S. pistillata* but not *A. yongei*. These differences indicate that these two coral species utilize distinct pathways to deliver ions to the sites of calcification and photosynthesis. Finally, antibodies against mammalian sodium bicarbonate cotransporters (NBC; SLC4 family) resulted in strong immunostaining in the apical membrane of oral epithelial cells and in calicoblastic cells in *A. yongei*, a pattern identical to NKA. Characterization of ion transport mechanisms is an essential step toward understanding the cellular mechanisms of coral physiology and will help predict how different coral species respond to environmental stress.

sodium pump; calcium pump; bicarbonate transporter; SLC4; ATPase

CORAL REEF ECOSYSTEMS ARE impacted by a variety of local and global stressors. Eutrophication and sedimentation from coastal development affect coral growth, reproduction, and survival (11); rising sea surface temperatures have led to an increase in coral mortality through the breakdown of symbiosis between corals and their intracellular dinoflagellate algae, a phenomenon known as coral bleaching (22, 56); and ocean acidification driven by dissolution of CO_2 in the ocean is predicted to impede coral calcification (14, 15, 55). The effects of these stressors on coral physiology are complex and can be challenging to disentangle since they cooccur on many reefs and not all species respond similarly. Unfortunately, the lack of knowledge about the fundamental mechanisms of coral cell physiology limits our ability to understand the biological mechanisms driving coral stress responses, which, in turn, limits our ability to predict how corals will respond and adapt to environmental changes. This information is needed to help guide informed reef management decisions, making characterization of the cellular mechanisms driving coral responses to stressors crucial.

The transport of ions across the plasma membrane is a fundamental aspect of cell and epithelial physiology and requires a significant amount of metabolic energy (30). In corals, ion transport is critical for the uptake of ions from the surrounding seawater and their transport to the sites of calcification and photosynthesis (1, 8). During calcification, calcium ions (Ca^{2+}) and dissolved inorganic carbon (DIC) must traverse two (if coming from the coelenteron) or four (if coming from seawater) tissue layers (Fig. 1) to reach the subcalicoblastic space where $CaCO_3$ precipitation occurs (1). Although both paracellular and transcellular transport is likely involved, their relative contributions are not known. Similarly, DIC used for photosynthesis must be transported across the oral ectoderm to the gastrodermal cells, where the endosymbiotic algae reside (8). The transport of compounds originating within coral tissues, such as metabolic CO_2 and nitrogenous waste, is also critical, as they may be recycled within the symbiosis (8).

Despite the clear importance of ion transport in coral physiology, our knowledge of the proteins involved and their regulation is limited. In this study, we utilized immunohistochemistry to describe and compare the localization of three ion-transporting proteins that likely play a significant role in coral physiology: the Na^+/K^+-ATPase (NKA), the plasma membrane Ca^{2+}-ATPase (PMCA), and putative bicarbonate transporters from the SLC4 family, in two distantly related species of branching scleractinian corals: *Acropora yongei*, from the complex clade, and *Stylophora pistillata*, from the robust clade (4). These two clades diverged ~250–400 million years ago (Ma) (40, 47) and are hypothesized to have independently evolved calcification (40). This ancient divergence has likely led to the evolution of distinct physiological mechanisms, a hypothesis that we explore here.

NKA is one of the most important ion transporters in biology, and it uses energy from ATP hydrolysis to export three Na^+ across the cell membrane in exchange for the uptake of two K^+ (35). This activity generates an electrochemical gradient across the cell membrane that can be used to promote a variety of cellular processes, including the secondary transport of ions (e.g., H^+, HCO_3^-, Ca^{2+}, Cl^-, PO_4^{2-}, SO_4^{2-}), water, and nutrients (e.g., amino acids, glucose), formation of action potentials, intercellular signaling, and cell volume regulation (3, 35). NKA may consume a significant portion of an organism's energy budget, ranging from 20% of cellular ATP in mammals (44) to as much as 80% in developing sea urchins (21). However, despite the fundamental role of NKA in epithelial physiology, little is known about its localization or physiological role(s) in corals. Relatively more data, although

Address for reprint requests and other correspondence: Corresponding author: Martin Tresguerres, Scripps Institution of Oceanography, Univ. of California San Diego, La Jolla, CA 92093 (e-mail: mtresguerres@ucsd.edu).

 0363-6119/15 Copyright © 2015 the American Physiological Society

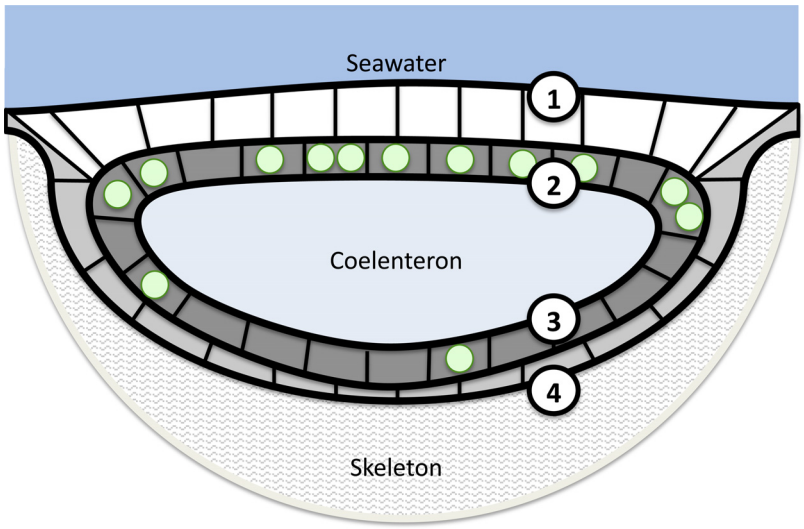

Fig. 1. Diagram of coral tissue structure. The oral ectoderm (1) lines the surface of the coral and is connected to the oral gastroderm (2) via an acellular matrix termed the mesoglea. The oral gastroderm (2) is where the majority of the endosymbiotic algae (circles) reside. The oral cell layers are separated from the aboral layers by the coelenteron. The aboral gastroderm (3) faces the coelenteron, and is connected via the mesoglea to the aboral (calicoblastic) ectoderm (4), which is in contact with the skeleton.

still scarce, are available for coral PMCA, which is hypothesized to play a role in coral calcification by serving as the main mechanism for the delivery of Ca^{2+} to the site of calcification (1, 8, 57). Furthermore, since PMCAs typically exchange Ca^{2+} for H^+ (5), this protein may also contribute to the maintenance of elevated pH in the subcalicoblastic space by removing protons generated during calcium carbonate precipitation (8, 57). PMCA mRNA is found throughout coral tissues, including the calicoblastic epithelium (57); however, the localization of the PMCA protein has not yet been determined. Finally, little is known about the identity or localization of proteins that deliver DIC to the sites of calcification and photosynthesis. On the basis of other ion-transporting epithelia, members of the SLC4 family are plausible candidates to mediate DIC transport in corals. For example, human SLC4A1-10 are able to transport HCO_3^- across cell membranes, and SLC4A4 and A5 may also transport CO_3^{2-} (41). Here, we used heterologous antibodies against rat SLC4A4, an electrogenic Na^+/HCO_3^- cotransporter (NBC), as a first step to localize potential DIC-transporting proteins in corals.

MATERIALS AND METHODS

Corals. Acropora yongei and *Stylophora pistillata* colonies were maintained in flow-through seawater aquaria under a 12:12-h light-dark cycle at 26°C. Colonies were sampled during the light for all experiments.

Tissue ultrastructure via TEM. A. yongei fragments were fixed overnight at 4°C in 2% paraformaldehyde and 2.5% glutaraldehyde in S22 buffer (37). Corals were then decalcified in Ca-free S22 with 0.5% paraformaldehyde at 4°C. Decalcification buffer was replaced daily for ~1–2 wk until the skeleton had completely dissolved. Fixed and decalcified coral tissue samples were immersed in modified Karnovsky's fixative (2.5% glutaraldehyde and 2% paraformaldehyde in 0.15 M sodium cacodylate buffer, pH 7.4) for at least 4 h, postfixed in 1% osmium tetroxide in 0.15 M cacodylate buffer for 1 h, and stained en bloc in 2% uranyl acetate for 1 h. Samples were dehydrated in ethanol, embedded in Durcupan epoxy resin (Sigma-Aldrich, St. Louis, MO), sectioned at 50 to 60 nm on a Leica UCT ultramicrotome, and picked up on Formvar and carbon-coated copper grids. Sections were stained with 2% uranyl acetate for 5 min and Sato's lead stain for 1 min. Grids were viewed using a JEOL 1200EX II (JEOL, Peabody, MA) transmission electron microscope and photographed using a Gatan digital camera (Gatan, Pleasanton, CA).

Primary antibodies. Commercially available primary antibodies used in this study included rabbit polyclonal anti-Na^+/K^+-ATPase α-subunit (NKA) antibodies raised against the mammalian protein (Santa Cruz Biotechnology, Santa Cruz, CA), rabbit polyclonal anti-rat NBC antiserum (Chemicon International, Temecula, CA), described in (42), and the mouse monoclonal antibody (anti-OxPhos) raised against human mitochondrial complex IV, subunit 1 (Invitrogen, Carlsbad, CA). This latter antibody has been shown to specifically label mitochondria in a variety of vertebrate and invertebrate animals (e.g., 48), and in our hands, it works in paraffin-embedded shark gill samples (39). Conservation of the epitopes recognized by the antibodies used throughout animal phyla, including corals, is shown in Table 1. Custom polyclonal rabbit antibodies were raised against a conserved region of the predicted coral PMCA protein from the *A. digitifera* genome (43); these antibodies were antigen-affinity

Table 1. *Comparison of protein sequence similarities between the immunogens against which the antibodies were designed and target proteins in Acropora spp. and Stylophora pistillata*

Target Protein	Immunogen	Immunogen Size, aa	*Acropora* Immunogen % Identical, (% Similar)	*Stylophora* Immunogen % Identical (% Similar)
Na^+-K^+ ATPase (α subunit)	aa 551–850 of human NKAα1 #	300	87% (97%)	87% (97%)
Na^+/HCO_3^- Cotransporter (SLC4A4)	aa 338–391 of rat kidney NBC #	54	42% (66%)	
Plasma membrane Ca^{2+}-ATPase	EKGIGGFPEDLDNR*	14	100%	71% (93%)
Cytochrome-*c* oxidase (mitochondrial complex IV)	Human cytochrome-*c* oxidase subunit 1 #	513	70% (83%)	73% (87%)

An asterisk (*) denotes custom-made antibodies, while # denotes commercially available antibodies. aa, amino acids.

purified. The full-length *S. pistillata* PMCA protein sequence (57) shares 81% identity with the predicted *Acropora* sequence, and the epitope region shares 71% identity (10/14 amino acids), with an additional 3 of the remaining 4 amino acids similar between the two species (93% similarity; 13/14 amino acids) (Table 1).

Molecular phylogeny analysis of coral Slc4-like proteins. Coral sequences JR988464, GASU01085070, aug_v2a.05797.t1, and aug_v2a.04799.t1; human SLC4s (41), zebrafish SLC4a4 (AAI62559.1) and SLC4a5 (XP_009299842.1), *Aedes aegypti* mosquito SLC4-like *Ae*AE (EU700988) and *Ae*NDAE (ACH96582) (36), diatom *Thalassiosira pseudonana* SLC4-like (XP_002286207.1) (32), and *Arabidopsis thaliana* SLC4-like (NP_172999.1) were aligned using MUSCLE (10) and analyzed using maximum likelihood on RAxML (46) and the model PROTCATWAG with 100 bootstraps; rooted to the *A. thaliana* protein sequence.

Western blot analysis of protein expression. Corals were homogenized in S22 buffer (37) supplemented with a protease inhibitor cocktail (Sigma) and phosphatase inhibitor (PhosStop; Roche Applied Science). Coral tissue was removed from the skeleton and homogenized using an airbrush (80 psi), and then it was passed through a 21 G syringe to shear the mucus. Samples were processed immediately or stored at −80°C. Protein concentrations for all samples were determined using the Bradford assay. Homogenates were incubated in Laemmli sample buffer with 5% B-mercaptoethanol for 15 min (NKA and PMCA: room temperature; NBC: 70°C), and then loaded on an SDS-PAGE gel (10–20 μg total protein in each lane). Following gel separation, proteins were transferred to a PVDF membrane using a TurboBlot (Bio-Rad, Hercules, CA). Membranes were blocked for 1 h on an orbital shaker in Tris-buffered saline with 0.1% Triton-X (TBS-T) with 5% fat-free milk at room temperature, and then incubated overnight at 4°C with the primary antibody (anti-NKA, 1:5,000 = 0.04 μg/ml; anti-PMCA, 1:500 = 0.625 μg/ml; anti-NBC, 1:500). The membrane was washed three times in TBS-T for 10 min each, and then stained with the secondary antibody (goat anti-rabbit-HRP; Bio-Rad) for 1 h at room temperature with shaking. The membrane was washed again, and bands were visualized using the ECL Prime Western blot detection reagent (GE Healthcare, New York, NY), and then imaged in a Bio-Rad Chemidoc Imaging system.

Immunofluorescence localization. Four 2–3-cm fragments of each coral species were prepared as described in Ref. 37. Briefly, samples were fixed overnight in S22 buffer (450 mM NaCl, 10 mM KCl, 58 mM $MgCl_2$, 10 mM $CaCl_2$, 100 mM HEPES, pH 7.8) with 3% paraformaldehyde at 4°C. Corals were then decalcified in Ca-free S22 buffer with 0.5 M EDTA at 4°C, and the buffer was replaced daily until the skeleton was completely dissolved (~7–10 days). Tissue was then dehydrated, embedded in paraffin, and sectioned into 7-μm sections. Tissue sections were rehydrated, blocked for 1 h with normal goat serum in PBS, and stained with the primary antibody overnight at 4°C (dilutions: anti-NKA, 2 μg/ml; anti-OxPhos, 2 μg/ml; anti-PMCA, 1.25 μg/ml; anti-NBC, 1:100). Sections were incubated with the appropriate secondary antibody (goat anti-rabbit-Alexa Fluor 555 or goat anti-mouse Alexa Fluor 555, 4 μg/ml; Invitrogen), and stained with Hoechst (1 μg/ml) for 5 min at room temperature to visualize DNA. Controls were treated as above, except no primary antibody was used. Stained tissue sections were visualized using a fluorescence microscope (Zeiss AxioObserver). Control images were taken with the same exposure settings used for the corresponding treatment. For each set of antibodies, at least two tissue sections from each coral branch were immunostained and analyzed (with the exception of the anti-OxPhos antibody, which was studied in six sections from three branches). Tissue sections analyzed for this study avoided the first ~1 cm of the branch tip to compare physiologically similar regions between colonies and between species. Observations of paraffin sections from branch tips did not reveal any obvious difference in immunostaining patterns for any of the antibodies. Similarly, all localizations presented here are from the coenosarc region because all four coral tissue layers are readily identifiable in this region.

Immunogold localization. A. yongei fragments were fixed overnight at 4°C in 4% paraformaldehyde in S22 buffer (37). Corals were then decalcified as described above. Fixed tissue was then washed with 0.15 M glycine/phosphate buffer, embedded in 10% gelatin/phosphate buffer and infused with 2.3 M sucrose/phosphate buffer overnight at 4°C. One cubic millimeter cell blocks were mounted onto specimen holders and snap frozen in liquid nitrogen. Ultracryomicrotomy was carried out at −100°C on a Leica Ultracut UCT with EM FCS cryoattachment (Leica, Bannockburn, IL) using a Diatome diamond knife (Diatome US, Hatfield, PA). Frozen sections (90 nm for TEM or 400 nm for immunofluorescence) were picked up with a 1:1 mixture of 2.3 M sucrose and 2% methyl cellulose (15cp), as described by Liou et al. (25), and transferred onto Formvar and carbon-coated copper grids. Immunolabeling was performed by a slight modification of the "Tokuyasu technique" (53). Briefly, grids were placed on 2% gelatin at 37°C for 20 min and rinsed with 0.15 M glycine/PBS; the sections were blocked using 1% cold water fish-skin gelatin. Previously titrated primary antibodies were diluted in 1% BSA/PBS. Incubation with primary antibodies for 1 h at room temperature was followed by gold conjugated goat anti-rabbit IgG, diluted 1:25 in 1% BSA/PBS, at room temperature for 30 min. Grids were viewed using a JEOL 1200EX II (JEOL, Peabody, MA) transmission electron microscope and photographed using a Gatan digital camera (Gatan), or viewed using a Tecnai G2 Spirit BioTWIN transmission electron microscope equipped with an Eagle 4k HS digital camera (FEI, Hilsboro, OR).

ATPase assays. Five 2–3-cm fragments of *A. yongei* were collected from a single parent colony, flash frozen in liquid nitrogen, and stored at −80°C. Tissue was removed from the skeleton and homogenized on ice using an airbrush (75 psi) with ~4 ml of homogenization buffer (50 mM imidazole, pH 7.5, containing 1× protease inhibitor cocktail [Sigma] and 1× PhosSTOP [phosphatase inhibitor cocktail, Roche Life Sciences]). Tissue homogenates were passed through a 19½ gauge needle using a syringe to shear the mucus, then sequentially filtered through a 100-μm mesh filter followed by a 40-μm mesh filter to remove any remaining mucus strands and skeleton fragments. Filtered homogenates were then centrifuged for 20 min at 20,000 *g* and 4°C to pellet the insoluble material and zooxanthellae, and protein content for each homogenate was determined by the Bradford method. Tissue homogenates were assayed for ATPase activity the same day or immediately frozen at −80°C and assayed within 7 days to minimize protein degradation.

The total ATPase activity was measured using a protocol similar to that presented by McCormick in 1993 (29) and optimized for corals. The assay is based on the enzymatically coupled hydrolysis of ATP and the oxidation of NADH. ATPase activity was assayed under four different conditions: control, 1 mM ouabain, 5 mM ouabain, or K^+-free. Each treatment was run in duplicate for each coral homogenate. The first assay mixture, solution A, was prepared containing 4 U lactate dehydrogenase/ml, 5 U pyruvate kinase/ml, 2.8 mM phosphoenolpyruvate, 0.7 mM ATP, 0.22 mM NADH, and 50 mM imidazole (pH 7.5). Two additional assay mixtures, solutions B and C, were prepared by supplementing solution A with either 1 mM or 5 mM ouabain, respectively. The assay solutions were used within 3 days of preparation to minimize enzymatic degradation. A normal salt solution was prepared containing (in mM) 189 NaCl, 10.5 $MgCl_2$, 42 KCl, and 50 imidazole (pH 7.5). Finally, a K^+-free salt solution was prepared containing (in mM) 189 NaCl, 10.5 $MgCl_2$, and 50 imidazole (pH 7.5). Salt solutions were used within 2–3 wk of preparation. Assay solutions were mixed in a 3:1 ratio with the salt solutions in the following combinations: solution A + normal salt solution, solution A + K^+-free salt solution, solution B + normal salt solution, and solution C + normal salt solution.

Coral homogenates were thawed on ice prior to the assay, and 40 μl was added to each sample well of a 96-well microplate kept on ice. Negative controls were obtained by boiling aliquots of each coral homogenate at 100°C for 10 min and run in duplicate alongside

normal homogenates. A standard curve was run in duplicate by adding 10 μl of freshly made ADP standards to achieve final concentrations of 0, 5, 10, 15, or 20 nmol ADP/well instead of the homogenates. Coral homogenates, standards, and the 3:1 assay-salt solution mixtures were brought to the assay temperature (25°C) for 5 min. To initiate the reaction, 170 μl of the appropriate 3:1 assay-salt solution was added to each sample, and 200 μl of the 3:1 control assay-salt solution was added to each standard for final volumes of 210 μl/well. The absorbance at 340 nm was read every 7 s for 10 min for samples and 7 min for standards using a SpectraMax M2 Microplate Reader with controlled temperature set at 25°C.

Total ATPase activity was calculated as the rate of ADP production in $\mu mol \cdot mg^{-1} \cdot$protein h^{-1}, using the following equation: $[(\Delta Abs/h)/(\varepsilon \cdot L)] \cdot [V(rxn)/V(ch)] \cdot (1/C)$, where $\Delta Abs/h$ is the change in absorbance per hour and was calculated by taking the slope of the change in NADH absorbance over the steepest part of the reaction curve (ΔOD/h), ε is the extinction coefficient (6.22 mM/cm for NADH, L is the pathlength of the reaction in the microplate well), $V(rxn)$ is the volume of the reaction in each plate well, $V(ch)$ is the volume of the crude homogenate, and C is the protein concentration of the homogenate (mg/ml).

RESULTS

A. yongei ultrastructure. Septate junctions were observed in the apico-lateral membrane of cells from all four coral cell layers: oral ectoderm (Fig. 2*A*), oral gastroderm (Fig. 2*B*), aboral gastroderm (Fig. 2, *C* and D), and calicoblastic ectoderm (Fig. 2, *C* and *D*). Intact vesicles were also observed within calicoblastic cells, as well as vesicles in the process of endocytosis or exocytosis (Fig. 2*D*), which suggest a transcellular mechanism for transporting molecules for calcification.

Localization of mitochondrion-rich cells in A. yongei. We found that using TEM, mitochondria were readily visible in cells from all tissue layers from *A. yongei* (Fig. 2), including but not limited to nematocysts and other cells in the oral ectoderm (Fig. 2*A*), oral gastrodermal cells with and without *Symbiodinium* (Fig. 2*B*), aboral gastrodermal cells (Fig. 2*C*), and cells in the calicoblastic epithelium (Fig. 2, *C* and *D*). However, since TEM observations are restricted to a very narrow field of view, it does not allow a general appreciation of mitochondrial abundance in coral tissues. Microscopy on paraffin-embedded coral sections help circumvent this problem, as larger fields of view can be examined (Fig. 3). Immunostaining using antibodies against mitochondrial complex IV demonstrated that cells with large numbers of mitochondria were, indeed, abundant throughout all layers of *A. yongei* (Fig. 3*B*). While the presence of mitochondria throughout the coral epithelia is to be expected, their subcellular localization and regions of relatively high abundance may provide insight into the energetic demands of the different cell types. In the oral ectoderm, high concentrations of mitochondria were present at the base of nematocysts but also throughout other unidentified cell types (Fig. 3*B*). Large numbers of mitochondria were generally found in the apical (coelenteron-facing) region of cells that did not contain *Symbiodinium* in both the oral and aboral gastroderm (Fig. 3, *B* and *C*). Mitochondria present in symbiont-containing cells may serve as a source of CO_2 for photosynthesis

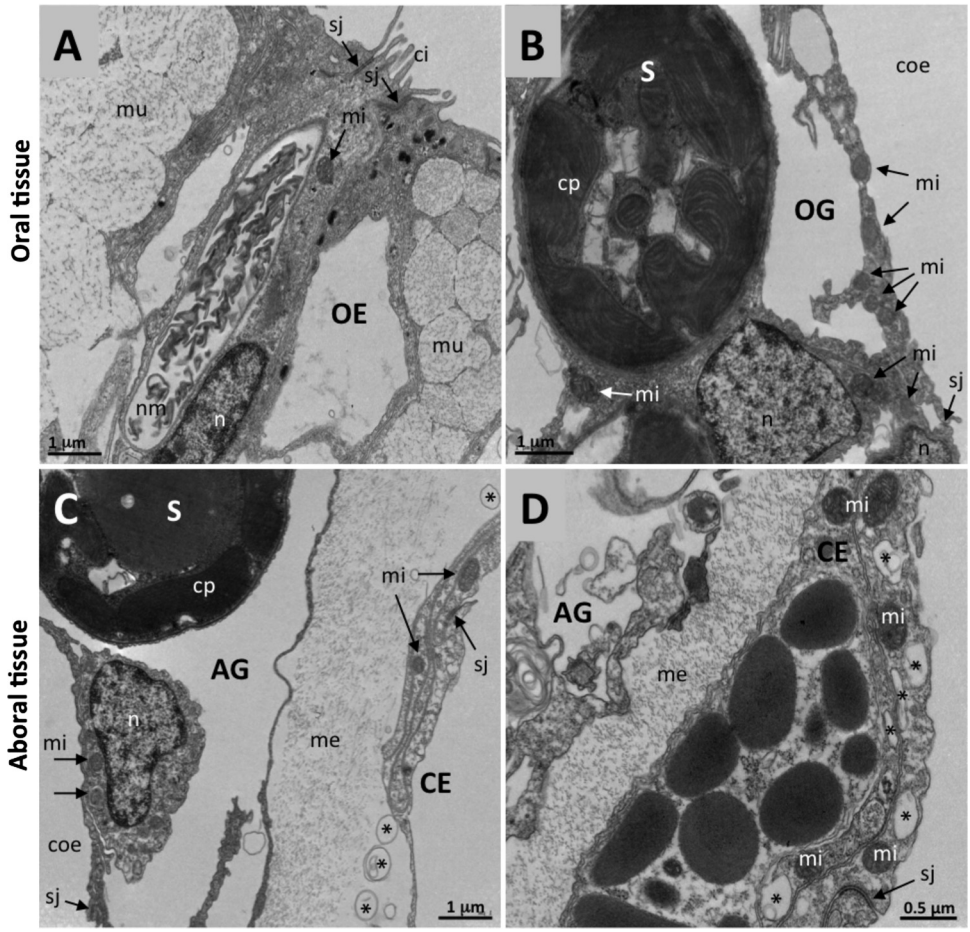

Fig. 2. Mitochondria and septate junctions in the oral (*A* and *B*) and aboral (*C* and *D*) tissue of *Acropora yongei*. Asterisks indicate vesicles. AG, aboral gastroderm; CE, calicoblastic ectoderm; OE, oral ectoderm; OG, oral gastroderm; S, *Symbiodiunium*; ci, cilia; coe, coelenteron; cp, chloroplast; me, mesoglea; mi, mitochondrion; mu, mucocyte; n, nucleus; nm, nematocyst; sj, septate junction.

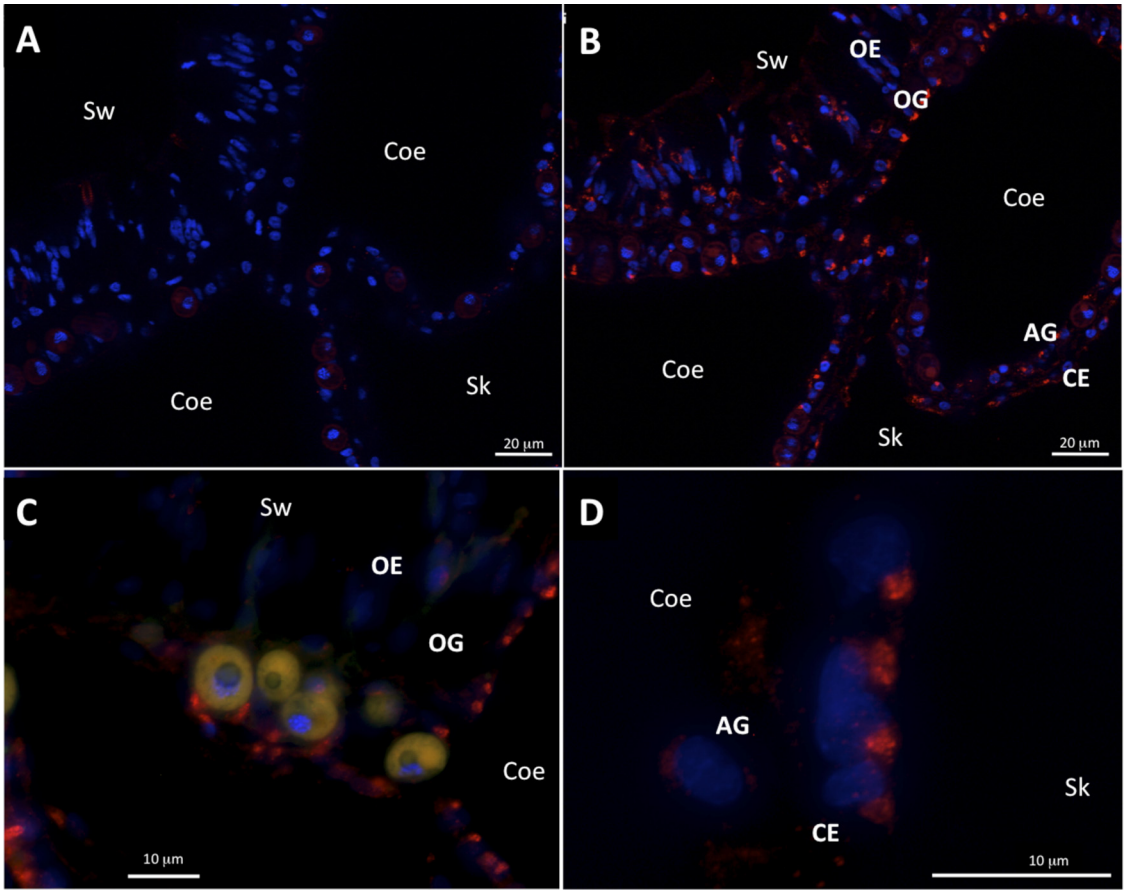

Fig. 3. Immunofluorescence localization of mitochondria with the anti-OxPhos antibody (red) in *A. yongei*. *A*: negative control (omission of primary antibody). *B*: low-magnification image showing abundant mitochondria (red) throughout coral tissues. *C*: detail of oral tissue, showing endogenous green fluorescence from *Symbiodinium* chlorophyll. *D*: detail of aboral tissue. Nuclei were stained with Hoechst (blue). AG, aboral gastroderm; CE, calicoblastic ectoderm; OE, oral ectoderm; OG, oral gastroderm; coe, coelenteron; Sk, skeleton; Sw, seawater.

(Fig. 3, *B* and *C*). Most cells in the calicoblastic ectoderm seemed to have a large amount of mitochondria (Fig. 3, *B* and *D*); these cells are very thin, so no particular polarity in the localization of mitochondria was evident.

Characterization of antibodies. Western blot with anti-NKA polyclonal antibodies yielded a single ~110-kDa band both in *A. yongei* and in *S. pistillata* (Fig. 4*A*), which is the predicted size for the NKA α-subunit in corals and most other species.

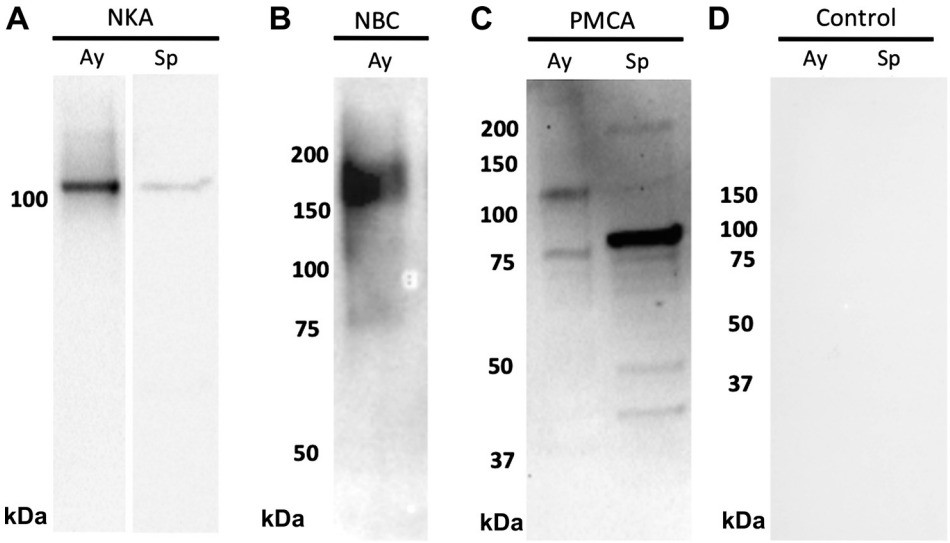

Fig. 4. Western blots against total protein for *A. yongei* (Ay) and *Stylophora pistillata* (Sp) using anti-NKA antibodies, (*A*) anti-SLC4-like protein(s) antibodies (Ay only) (*B*), anti-PMCA antibodies (*C*), and control using anti-PMCA antibodies (*D*) incubated overnight with 200-fold excess antigen peptide.

The anti-PMCA polyclonal antibodies yielded a strong ~130-kDa band in *A. yongei*, as well as a fainter band at ~75 kDa (Fig. 4*C*). In *S. pistillata*, these antibodies recognized a strong band of ~80 kDa, a few much fainter bands, including one at ~130 kDa, were also observed (Fig. 4*C*). BLAST searches using the epitope recognized by the anti-PMCA antibodies yielded only putative coral PMCAs as "hits": *A. cervicornis* (GASU01015145), *A. millepora* (JR973799.1; JT000352.1), and *S. pistillata* (AY360080.1, GARY01009939). Importantly, these predicted coral PMCAs have different molecular weights that range from ~127 kDa (*A. cervicornis* GASU01015145; *S. pistillata* AY360080.1) to ~70 kDa (*S. pistillata* GARY01009939), but the overlapping amino acid sequences of these proteins are virtually identical to each other. Altogether, these results suggest corals have multiple PMCA isoforms that are recognized by the antibodies.

The anti-rat NBC antisera recognized a ~180-kDa band in *A. yongei* (Fig. 4*B*), which is greater than the ~130-kDa band detected in rat and rabbit kidney but similar to the ~160-kDa band detected in salamander kidney (42). BLAST searches using the antigen epitope against coral genomic and transcriptomic databases yielded only putative SLC4s as "hits" (*A. millepora* = JR988464; *A. cervicornis* = GASU01085070; *A. digitifera* = aug_v2a.05797.t1; aug_v2a.04799.t1). On the basis of the size of the band in Western blots, the most likely candidates are the proteins encoded by aug_v2a.04799.t1 (predicted to encode a 127-kDa protein) and JR988464.1 (134-kDa protein). Furthermore, the antigen epitope is better conserved in the protein encoded by JR988464.1. Molecular phylogeny analysis revealed that this protein is most closely related to Na^+-dependent SLCs (100/100 bootstrap score with human SLC4A7, SLC4A8, and SLC4A10, and mosquito SLC4-like *Ae* NDAE), while the protein encoded by aug_v2a.04799.t1 is most closely related to anion exchangers (97/100 bootstrap score with human SLCA1, SLCA2, and SLCA3, and mosquito SLC4-like *Ae* AE). However, further experiments are required to definitively identify the immunolabeled coral protein(s), and, therefore, this is referred to as the "SLC4-like protein(s)". As proposed for salamander kidney NBC (42) and for mosquito *Ae*AE (36), the higher apparent molecular weight in Western blots is likely explained by glycosylation of coral SLC4-like protein(s). Unfortunately, the manufacturer of the anti-rat-NBC antibodies discontinued this product before we were able to optimize Western blots for *S. pistillata*. Therefore, immunolocalization studies were only conducted for *A. yongei*.

Western blot and immunohistochemistry (IHC) controls were performed for our custom anti-PMCA antibodies, including overnight preabsorption of the antibodies with 200-fold excess of the antigen peptide or incubation of the sample with the preimmune serum instead of the primary antibodies. All controls showed no staining; representative Western blots are shown in Fig. 4*D*, and IHC in Fig. 5. Our results indicate that the antibodies used in this study specifically recognize the respective coral proteins.

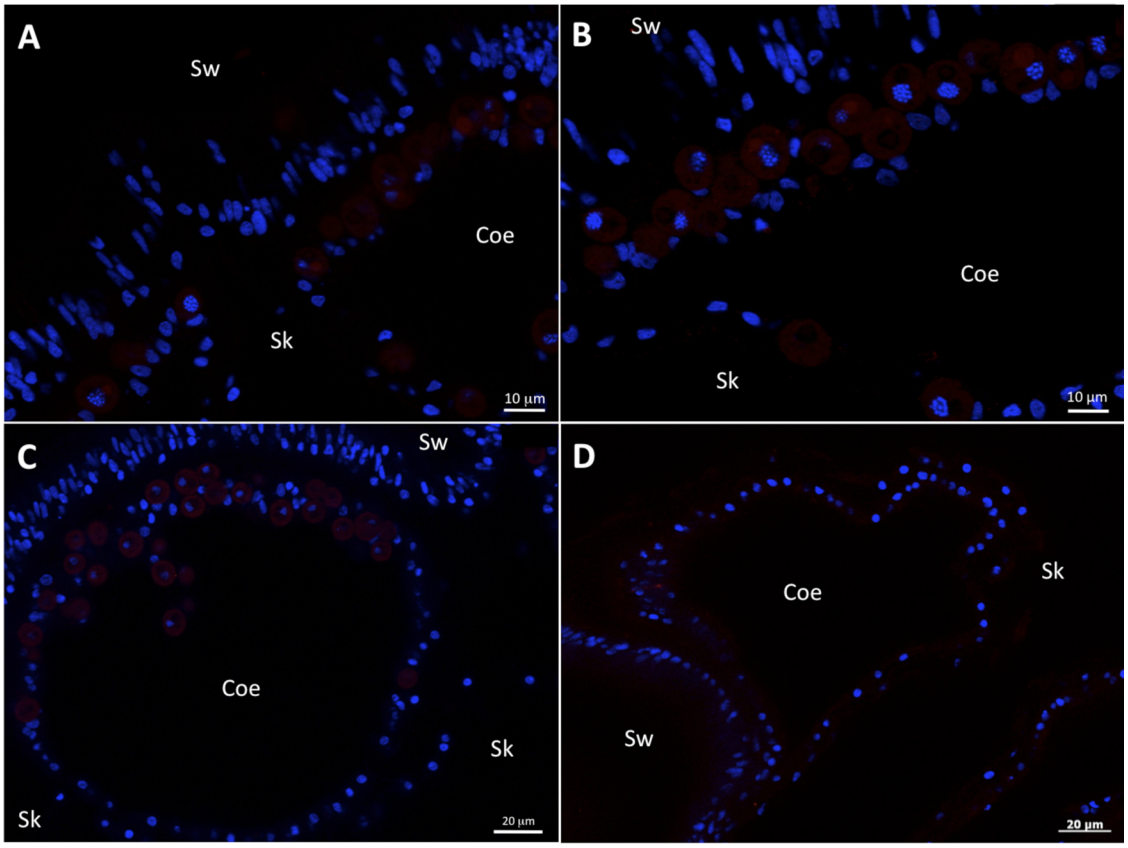

Fig. 5. Immunohistochemistry controls for the custom anti-PMCA antibodies for *A. yongei* (*top*) and *S. pistillata* (*bottom*). *A* and *C*: samples were incubated with the preimmune serum followed by the secondary antibodies (red). *B* and *D*: anti-PMCA antibodies were incubated overnight with 200-fold excess antigen peptide prior to IHC, followed by the secondary antibodies (red). Nuclei were stained with Hoechst (blue). Sw, seawater side; Coe, coelenteron, Sk, skeleton side.

Localization of ion transport proteins in A. yongei. Immunofluorescence localization demonstrated that NKA was abundant in the oral and calicoblastic ectoderm (Fig. 6*A*). In the calicoblastic ectoderm, NKA was restricted to the basolateral membrane (Fig. 6*B*), whereas in the oral ectoderm, NKA was found in the apical membrane, including microvilli lining the outer surface of the coral (Fig. 6*A*). Since localization of NKA in the apical membrane is unusual, its subcellular localization was further determined by immuno-TEM, which confirmed NKA was present in apical microvilli (Fig. 6*C*). Coral SLC4-like protein(s) followed a similar localization pattern as NKA (Fig. 6*D*): in the calicoblastic ectoderm, it appeared in the basolateral membrane (Fig. 6*E*), while in the oral ectoderm, it was in the apical membrane, including apical microvilli (Fig. 6*F*). However, unlike NKA, SLC4-like protein(s) was also found in the apical membrane of some calicoblastic cells. PMCA was present in all tissue layers (Fig. 6*G*), although it was most abundant in the cytoplasm of calicoblastic cells (Fig. 6*H*) and the apical pole of cells in the oral ectoderm (Fig. 6*G*). Unlike NKA and SLC4-like protein(s), PMCA was not observed in apical microvilli lining the surface of the oral ectoderm (Fig. 6*I*), suggesting that it is not in the plasma membrane of these cells.

ATPase activity assays using *A. yongei* tissue homogenates indicated that NKA activity, as estimated from the fraction of total ATPase activity inhibited under K^+-free conditions, was 13.5 ± 1.4% of the total ATPase activity (Table 2, $P < 0.05$, $n = 5$). Ouabain, a traditional NKA inhibitor in other organ-

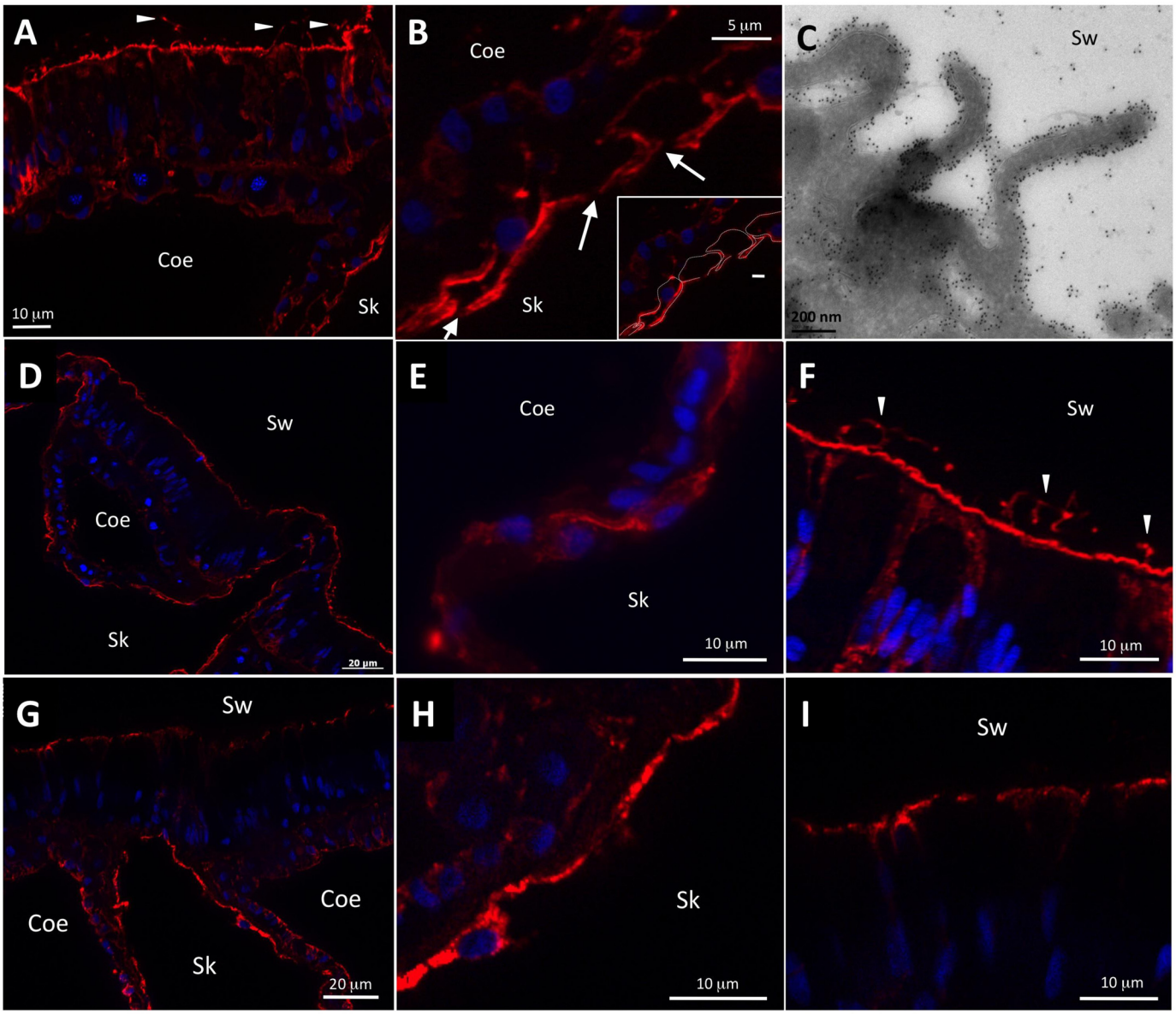

Fig. 6. Immunolocalization of the Na^+/K^+-ATPase (NKA), SLC4-like protein(s), and a plasma membrane Ca^{2+}-ATPase (PMCA) in *A. yongei*. *A–C*: anti-NKA antibodies (red), immuno-transmission electron microscopy (TEM) image of apical microvilli labeled with the anti-NKA antibodies (black dots: *C*). *D–F*: anti-SLC4-like proteins antibodies (red). *G–I*: anti-PMCA antibodies (red). Arrowheads indicate microvilli positive for NKA or SLC4-like protein(s); arrows indicate unlabeled apical region in calicoblastic cells. The thin dotted line in the inset of *B* outlines the basolateral membrane of an NKA-immunolabeled calicoblastic cell. Nuclei were stained with Hoechst (blue). Sw, seawater side; Coe, coelenteron, Sk, skeleton side.

Table 2. *Average ATPase activity of Acropora yongei total protein preparations*

	ATPase Activity, μmol ADP·mg^{-1} protein·hr^{-1} ± SE	Inhibition of Total Activity, %	Inhibition of K^+-Sensitive Activity, %
Total	0.0162 ± 0.0008		
K^+-dependent	0.0022 ± 0.0012	13.5 ± 1.4 *	100*
Ouabain-sensitive (1 mM)	0.0007 ± 0.0002	4.7 ± 1.6	31.6 ± 9.8
Ouabain-sensitive (5 mM)	0.0005 ± 0.0001	3.7 ± 1.4	23.1 ± 4.8

*Significant differences with control (column 3) or K^+-free (column 4) (one-way RM-ANOVA, Tukey's post hoc test, $P < 0.05$; $n = 5$).

isms, induced a slight but not significant reduction in ATPase activity when applied at 1-mM or 5-mM concentrations. Furthermore, the effect of ouabain on ATPase activity was significantly lower compared with K^+ removal, indicating that ouabain had no significant effect on NKA activity at these concentrations (Table 2, $P < 0.05$, $n = 5$).

Localization of ion transport proteins in S. pistillata. Similar to *A. yongei*, NKA was present in and restricted to the basolateral membrane of calicoblastic cells of *S. pistillata* (Fig. 7, *A* and *B*). However, in contrast to *A. yongei*, NKA was not evident in the apical membrane of oral tissues of *S. pistillata* (Fig. 7, *A* and *B*). In addition, PMCA was present throughout all cell layers in *S. pistillata* (Fig. 7*C*), and in contrast with *A. yongei*, was most abundant in the cytoplasm of gastrodermal cells in the subcellular region facing the coelenteron (Fig. 7, *C* and *D*).

DISCUSSION

Scleractinian corals comprise two monophyletic clades, Complexa and Robusta. These two clades diverged before the appearance of coral skeletons in the fossil record around 240 million years ago (Ma) (40) and may have diverged as early as 425 Ma (47), providing strong evidence that calcification evolved independently in each clade (40). This has important implications for the mechanisms of coral calcification and overall physiology, and our study clearly demonstrates that corals from these two groups possess several important physiological distinctions at the cellular level. However, similar studies on additional representatives of the two coral clades are required (including azooxanthellate species) to establish whether these differences apply to all representatives of Complexa and Robusta, or if they are species-specific differences. Also importantly, our observations were made in the coenosarc of coral samples taken at least 1 cm away from the coral branch

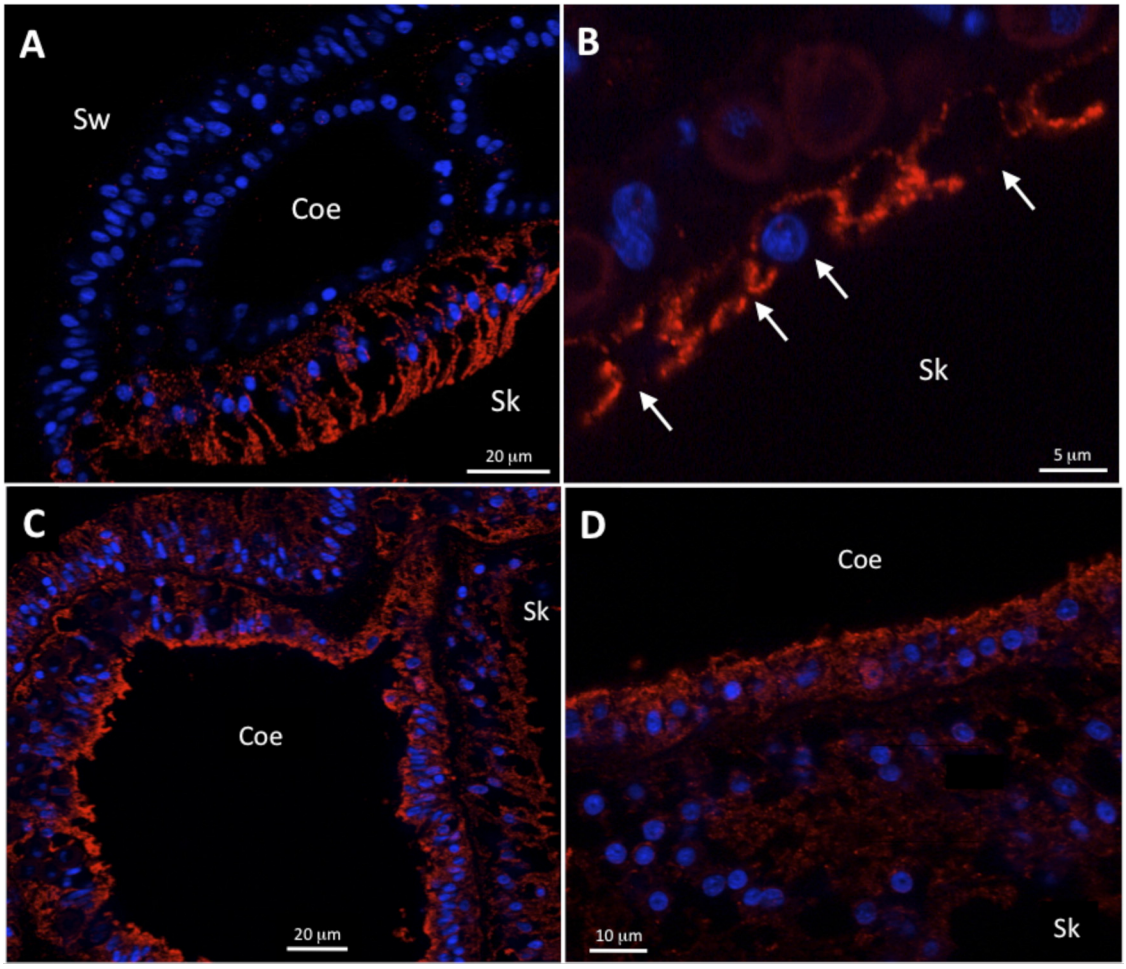

Fig. 7. Immunofluorescence localization of NKA and PMCA in *S. pistillata*. *A* and *B*: anti-NKA antibodies. *C* and *D*: anti-PMCA antibodies. Nuclei were stained with Hoechst (blue). Sw, seawater side; Coe, coelenteron; Sk, skeleton side.

tip. Since tips calcify at a more rapid rate and typically harbor fewer *Symbiodinium* algae (19), it is possible that they express a different subset of ion-transporting proteins. Similarly, the oral ectoderm of coral polyps may express another subset of proteins to transport DIC than the coenosarc. These are good examples of the complexity of coral biology, and a reminder that much caution must be used when interpreting "-omics" results from whole coral fragments, as the lack of information on basic coral cellular biology, cell types, and regional heterogeneity may result in incorrect and misleading conclusions about coral responses to environmental stress.

Morphological evidence of epithelial polarity and transcellular transport. Evidence of abundant vesicular transport across the calicoblastic epithelium in *A. yongei* was observed, with membrane fusion occurring on the apical and basal sides of the cells. This is in contrast to *S. pistillata*, where exocytotic vesicles were not observed (49), but it is consistent with previous reports from the robust coral *P. damicronis* (18) and the complex coral *A. hebes* (17). These vesicles may be a transcellular mechanism for the transport of Ca^{2+}, organic matrix, and other compounds across the calicoblastic cells in *A. yongei*, as reported in foraminifers (2, 33) and coccolitophores (26). Vesicular transport would have the benefit of sequestering Ca^{2+} away from the cytoplasm where its presence at high concentrations would be toxic. In further support of this hypothesis, rapidly calcifying regions have been found to contain higher abundances of vesicles in the calicoblastic cells of *A. hebes* (17).

The presence of junctions in an epithelium may seem trivial; however, their empirical demonstration in coral tissues is scarce. To our knowledge, this is the first report of septate junctions between cells across all the tissue layers of an Acropid coral. Septate junctions are intercellular junctions typical of invertebrate epithelial cells and play a key role in epithelial polarization. Septate junctions have previously been observed in the calicoblastic ectoderm of *S. pistillata* (49), *A. hebes* (17), *Pocillopora damicornis* (18), *Caryophyllia smithii* (52) and *Galaxaea fascicularis* (6), and a recent study reported septate junctions between cells of all germ layers in *S. pistillata* (12). In addition to determining epithelial polarization, intercellular junctions restrict the paracellular movement of ions across the epithelium and may also be involved in signaling pathways that regulate cell physiology and gene expression (28). Paracellular transport has been observed in *S. pistillata*; it allows the passage of the hydrophilic molecule calcein, and is selective for molecules between 13 Å and 20 nM in size (50). The permeability of *A. yongei* epithelia has not been tested, but septate junctions can also act like tight junctions by having differential permeability to certain ions and other molecules, and in some coral species or cell types, this may be the case (1, 6).

Ion transport mechanisms of the oral ectoderm. Contrary to its typical location in the basolateral membrane, NKA was found here in the apical membrane of the oral ectoderm of *A. yongei*, including microvilli. Though uncommon, this localization occurs in other epithelia; for example, in the microvilli of retinal pigment epithelial cells in vertebrates, NKA is involved in photoreception and maintenance of membrane polarization for neuronal sensing (34, 38), and in the apical membrane of the choroid plexus, NKA helps regulate fluid and pH balance (7). In corals, apical NKA may play similar roles, and in addition could energize the uptake of various ions and nutrients from the surrounding seawater such as Ca^{2+}, DIC, carbohydrates, and amino acids through the generation of electrochemical gradients. For example, the colocalization of SLC4-like protein(s) with NKA in *A. yongei* suggests that the SLC4-like protein(s) utilizes the Na^+ gradient generated by NKA to import HCO_3^- into the coral cytoplasm. The lack of NKA signal in the oral epithelium of *S. pistillata* suggests that this species utilizes a distinct suite of transporters to drive ion and nutrient transport, which may lead *S. pistillata* and *A. yongei* to exhibit distinct responses to changes in the surrounding environment, such as pH or the availability of organic and inorganic nutrients.

Because of moderate similarity of the region recognized by the antibodies within the putative coral SLC4 family, we cannot determine the specific coral SLC4 isoform(s) that was immunolabeled in *A. yongei*, or if multiple isoforms were immunolabeled. On the basis of higher homology of the antigen peptide sequence and molecular weight of the predicted protein, the best candidate is the protein encoded by JR988464.1, which is more closely related to human and mosquito Na^+-dependent SLC4s. However, further experiments, including cloning, characterization of substrate specificity, and localization using isoform-specific antibodies would be required to speculate about the physiological function of coral SLC4s.

PMCA was also found in the oral ectoderm of both coral species, although its localization differed. PMCA appeared throughout the cytoplasm in *S. pistillata*, but it was concentrated at the apical pole in *A. yongei*. PMCA was not observed in the basolateral plasma membrane of either species, suggesting that PMCA does not mediate Ca^{2+} absorption across the oral ectoderm, or that the oral ectoderm does not uptake Ca^{2+} from seawater. Previous gene expression studies have shown that *S. pistillata* expresses two different PMCA1 isoforms with predicted sizes of ~70 kDa (23) and ~127 kDa (57). The amino acid sequences for these two PMCA isoforms are identical, including the region encoding for the antigen recognized by our antibodies, and thus the localization patterns we observed may include two or more PMCA isoforms. Differential abundance of PMCA isoforms or splice variants between *A. yongei* and *S. pistillata* may explain the distinct cellular localization patterns. In any case, our immunolocalization results suggest that none of these putative PMCA variants are located directly in the cell membrane of ectodermal cells.

Ion transport in the gastroderm. The relatively high abundance of mitochondria in cells along the coelenteron of *A. yongei* suggests a high capacity for active solute transport. This region demonstrated some NKA immunostaining, although much weaker compared with ectodermal cells, as well as strong PMCA immunostaining. PMCA was observed in the cytoplasm of coral cells throughout the gastroderm of both species and was particularly abundant along the coelenteron-facing side of gastrodermal cells in *S. pistillata*. However, the absence of PMCA in gastrodermal cell membranes raises questions about whether it plays a role in transepithelial Ca^{2+} transport for calcification or if it is involved in maintaining intracellular Ca^{2+} homeostasis.

Evidence for conserved and distinct mechanisms of ion transport in the calicoblastic ectoderm. The presence of NKA in the basolateral membrane of calicoblastic cells in both *A.*

yongei and *S. pistillata* indicates that NKA is a conserved mechanism involved in coral calcification. Furthermore, this is the first study to demonstrate basolateral localization of a membrane protein in corals. The subcellular restriction of NKA in both species confirms that these cells are polarized, a critical feature for epithelial function as it allows for directional transport of ions across the tissue. NKA in calicoblastic cells could have multiple functions; for example, it likely helps transport HCO_3^-, Ca^{2+}, H^+, and organic matrix precursors across the basolateral membrane by secondary active transport. The colocalization of NKA with SLC4-like protein(s) in *A. yongei* supports this hypothesis, as NKA activity would secondarily energize the transport of HCO_3^-, CO_3^{2-}, and other molecules across apical and basolateral membranes. For example, the localization of SLC4-like transporters in the apical membrane of the calicoblastic cells suggests a mechanism for supplying the subcalicoblastic medium (SCM) with DIC for calcification and/or pH regulation. Furthermore, the abundance of mitochondria in the calicoblastic epithelium in both species is consistent with high ATP demand by NKA (and possibly other ATPases) and is also a likely source of DIC for calcification through the production of CO_2 during aerobic respiration.

PMCA was present in the cytoplasm of calicoblastic cells of both species, indicating that PMCA may be a mechanism for concentrating Ca^{2+} in intracellular vesicles for Ca^{2+} homeostasis or possibly for calcification. Our results disagree with the existing model proposing that PMCA1 is located in the apical membrane of calicoblastic cells and transports Ca^{2+} to the SCM for calcification (8, 57). However, this model is based on results from in situ hybridization (57), a technique that detects mRNA for the genes of interest in specific cells but does not provide any information about the subcellular localization of the protein. Similarly, Ca^{2+}-ATPase-like activity has been reported in membrane-enriched fractions from the coral *G. fascicularis* (16); however, the specific source of this activity (i.e., ectoderm or endoderm, oral or aboral, plasma membrane, or vesicles) could not be determined, preventing a conclusive determination of the physiological role of this activity.

Recent transcriptome analyses provide further support for the role of NKA in calcification. For example, expression of the NKA gene was increased in rapidly calcifying regions of the corals *A. cervicornis* and *A. palmata*, while levels of multiple PMCA trancripts remained constant (13). These data suggest that NKA activity helps drive coral calcification and further calls into doubt the presumed role of PMCA in calcification. In addition, NKA transcript was upregulated under high CO_2 conditions in *A. millepora* (20), suggesting that more metabolic energy is required to maintain calcification and/or nutrient and ion uptake from the seawater during ocean acidification. In contrast, the PMCA gene in both *S. pistillata* (54) and *A. millepora* (31) exposed to ocean acidification remained equivalent to controls, though it was down-regulated in *S. pistillata* exposed to extreme acidification (pH 7.2) (54). Given that our results show that PMCA protein is expressed throughout all coral layers but not in the plasma membrane of either *A. yongei* or *S. pistillata*, the actual function of PMCA isoforms and their physiological significance with respect to calcification remains to be studied.

To definitively assess the role of ion-transporting proteins in coral physiology, a method to specifically block their activities would be required. Unfortunately, gene silencing or knock down of specific genes has not yet been developed for corals, and pharmacological inhibitors, which are specific for mammalian transporters, do not necessarily have the same efficacy and specificity in corals. In this study, the NKA inhibitor ouabain did not significantly inhibit NKA activity in *A. yongei*, which raises questions on a previous report of 1 mM ouabain inhibiting light-dependent calcium uptake in corals (27). Was this effect due to NKA inhibition, or to unspecific effects on some other cellular component(s)? And if it were due to NKA inhibition, which pool was affected (e.g., oral vs. aboral ectoderm)? Since a fellow cnidarian, the sea anemone *Stichodactyla helianthus*, also has significantly reduced NKA-specific ouabain-sensitivity compared with rat NKA (45), it may be that cnidarians are not as sensitive to ouabain as other species. Another point to consider is the potential for differential properties of NKA catalytic α-subunit isoforms regarding ouabain sensitivity and tissue localization, as described in mammals (9). These examples illustrate the need for characterizing the effects of pharmacological inhibitors on the specific coral protein(s) and for a careful interpretation of results due to the potential for off-target effects.

Perspectives and Significance

This is the first study to localize ion transport proteins relevant for acid/base regulation and photosynthesis in corals and only the second study to show localization of a coral Ca^{2+}-transporting protein (58). The differential localization of ion transport proteins within different cell types or compartments within individual cells observed here may lead to a variety of cell- and tissue-specific responses (3) that would be missed by global or bulk mRNA and protein assessments. Additionally, the potential differences between robust and complex corals highlight the evolutionary divergence between these two clades of Scleractinia and the need for the identification of species-specific mechanisms. Future work is needed to determine the functional roles of ion transporters in corals, but this first requires characterizing their substrate specificity, kinetics, and pharmacology, as has been done for SLC4s in other organisms such as mammals (41), fish (51), and mosquito (24). The detailed description of ion transport mechanisms in corals is a fundamental step toward understanding and predicting general and species-specific responses of corals to the variety of environmental stressors they currently face on reefs around the world.

ACKNOWLEDGMENTS

We are grateful to Dimitri Deheyn and Jenny Tu for providing *Acropora yongei* specimens, Greg Rouse for help with phylogeny analysis, Fernando Nosratpour for *Stylophora pistillata* specimens, Jinae Roa and Yuzo Yanagitsuru for help with Western blots, and the University of California San Diego Electron Microscopy Facility for assistance with transmission electron microscopy.

GRANTS

This work was supported by the National Science Foundation Grants EF-1220641 to M. Tresguerres and OCE-1226396 to K. L. Barott, and by an Alfred P. Sloan Research Fellowship (Grant BR2013-103) to M. Tresguerres.

DISCLOSURES

No conflicts of interest, financial or otherwise, are declared by the authors.

AUTHOR CONTRIBUTIONS

Author contributions: K.L.B. and M.T. conception and design of research; K.L.B., S.O.P., and L.B.L. performed experiments; K.L.B., S.O.P., L.B.L., and M.T. analyzed data; K.L.B. and M.T. interpreted results of experiments; K.L.B. and M.T. prepared figures; K.L.B. and M.T. drafted manuscript; K.L.B., S.O.P., L.B.L., and M.T. edited and revised manuscript; K.L.B., S.O.P., L.B.L., and M.T. approved final version of manuscript.

REFERENCES

1. **Allemand D, Tambutté É, Zoccola D, Tambutté S.** Coral Calcification, Cells to Reefs [Online]. In: *Coral Reefs: An Ecosystem in Transition*, edited by Dubinsky Z, Stambler N. Rotterdam, The Netherlands: Springer Netherlands, p. 119–150. http://link.springer.com/chapter/10.1007/978-94-007-0114-4_9 [12 Sep. 2013].
2. **Bentov S, Brownlee C, Erez J.** The role of seawater endocytosis in the biomineralization process in calcareous foraminifera. *Proc Natl Acad Sci USA* 106: 21,500–21,504, 2009.
3. **Blanco G, Mercer RW.** Isozymes of the Na-K-ATPase: heterogeneity in structure, diversity in function. *Am J Physiol Renal Physiol* 275: F633–F650, 1998.
4. **Budd AF, Romano SL, Smith ND, Barbeitos MS.** Rethinking the phylogeny of Scleractinian corals: a review of morphological and molecular data. *Integr Comp Biol* 50: 411–427, 2010.
5. **Carafoli E.** The calcium pumping ATPase of the plasma membrane. *Annu Rev Physiol* 53: 531–547, 1991.
6. **Clode PL, Marshall AT.** Low temperature FESEM of the calcifying interface of a scleractinian coral. *Tissue Cell* 34: 187–198, 2002.
7. **Damkier HH, Brown PD, Praetorius J.** Epithelial pathways in choroid plexus electrolyte transport. *Physiology* 25: 239–249, 2010.
8. **Davy SK, Allemand D, Weis VM.** Cell biology of cnidarian-dinoflagellate symbiosis. *Microbiol Mol Biol Rev* 76: 229–261, 2012.
9. **Dostanic-Larson I, Lorenz JN, Van Huysse JW, Neumann JC, Moseley AE, Lingrel JB.** Physiological role of the alpha1- and alpha2-isoforms of the Na^+-K^+-ATPase and biological significance of their cardiac glycoside binding site. *Am J Physiol Regul Integr Comp Physiol* 290: R524–R528, 2006.
10. **Edgar RC.** MUSCLE: multiple sequence alignment with high accuracy and high throughput. *Nucleic Acids Res* 32: 1792–1797, 2004.
11. **Fabricius KE.** Effects of terrestrial runoff on the ecology of corals and coral reefs: review and synthesis. *Mar Pollut Bull* 50: 125–146, 2005.
12. **Ganot P, Zoccola D, Tambutté E, Voolstra CR, Aranda M, Allemand D, Tambutté S.** Structural molecular components of septate junctions in cnidarians point to the origin of epithelial junctions in eukaryotes. *Mol. Biol. Evol*. (September 21, 2014). doi: 10.1093/molbev/msu265.
13. **Hemond EM, Kaluziak ST, Vollmer SV.** The genetics of colony form and function in Caribbean *Acropora* corals. *BMC Genomics* 15: 1133, 2014.
14. **Hoegh-Guldberg O, Australia G.** Climate change, coral bleaching and the future of the world's coral reefs. *Mar Freshw Res* 50: 839–866, 1999.
15. **Hoegh-Guldberg O, Mumby PJ, Hooten AJ, Steneck RS, Greenfield P, Gomez E, Harvell CD, Sale PF, Edwards AJ, Caldeira K, Knowlton N, Eakin CM, Iglesias-Prieto R, Muthiga N, Bradbury RH, Dubi A, Hatziolos ME.** Coral reefs under rapid climate change and ocean acidification. *Science* 318: 1737–1742, 2007.
16. **Ip YK, Lim ALL, Lim RWL.** Some properties of calcium-activated adenosine triphosphatase from the hermatypic coral *Galaxea fascicularis*. *Mar Biol* 111: 191–197, 1991.
17. **Isa Y, Yamazato K.** The ultrastructure of calicoblast and related tissues in *Acropora hebes* (Dana). *Proc 4th Int Coral Reef Symp* 2: 99–105, 1981.
18. **Johnston IS.** The ultrastructure of skeletogenesis in hermatypic corals [Online]. In: *International Review of Cytology*, edited by G. H. Bourne and J. F. Danielli. San Diego, CA: Academic Press, p. 171–214. http://www.sciencedirect.com/science/article/pii/S0074769608624298 [19 Sep. 2013].
19. **Jokiel PL.** The reef coral two compartment proton flux model: A new approach relating tissue-level physiological processes to gross corallum morphology. *J Exp Mar Biol Ecol* 409: 1–12, 2011.
20. **Kaniewska P, Campbell PR, Kline DI, Rodriguez-Lanetty M, Miller DJ, Dove S, Hoegh-Guldberg O.** Major cellular and physiological impacts of ocean acidification on a reef building coral. *PLoS ONE* 7: e34659, 2012.
21. **Leong P, Manahan D.** Metabolic importance of Na^+/K^+-ATPase activity during sea urchin development. *J Exp Biol* 200: 2881–2892, 1997.
22. **Lesser MP.** Coral reef bleaching and global climate change: Can corals survive the next century? *Proc Natl Acad Sci* 104: 5259, 2007.
23. **Liew YJ, Aranda M, Carr A, Baumgarten S, Zoccola D, Tambutté S, Allemand D, Micklem G, Voolstra CR.** Identification of microRNAs in the coral *Stylophora pistillata*. *PloS One* 9: e91101, 2014.
24. **Linser PJ, Neira Oviedo M, Hirata T, Seron TJ, Smith KE, Piermarini PM, Romero MF.** Slc4-like anion transporters of the larval mosquito alimentary canal. *J Insect Physiol* 58: 551–562, 2012.
25. **Liou W, Geuze HJ, Slot JW.** Improving structural integrity of cryosections for Immunogold labeling. *Histochem Cell Biol* 106: 41–58, 1996.
26. **Mackinder L, Wheeler G, Schroeder D, Riebesell U, Brownlee C.** Molecular mechanisms underlying calcification in coccolithophores. *Geomicrobiol J* 27: 585–595, 2010.
27. **Marshall AT.** Calcification in hermatypic and ahermatypic corals. *Sci New Ser* 271: 637–639, 1996.
28. **Matter K, Balda MS.** Signalling to and from tight junctions. *Nat Rev Mol Cell Biol* 4: 225–236, 2003.
29. **McCormick SD.** Methods for nonlethal gill biopsy and measurement of Na^+, K^+-ATPase activity. *Can J Fish Aquat Sci* 50: 656–658, 1993.
30. **Milligan L, McBride B.** Energy costs of ion pumping by animal tissues. *J Nutr* 115: 1374–1382, 1985.
31. **Moya A, Huisman L, Ball EE, Hayward DC, Grasso LC, Chua CM, Woo HN, Gattuso JP, Forêt S, Miller DJ.** Whole transcriptome analysis of the coral *Acropora millepora* reveals complex responses to CO_2-driven acidification during the initiation of calcification. *Mol Ecol* 21: 2440–2454, 2012.
32. **Nakajima K, Tanaka A, Matsuda Y.** SLC4 family transporters in a marine diatom directly pump bicarbonate from seawater. *Proc Natl Acad Sci USA* 110: 1767–1772, 2013.
33. **De Nooijer LJ, Toyofuku T, Kitazato H.** Foraminifera promote calcification by elevating their intracellular pH. *Proc Natl Acad Sci USA* 106: 15374–15378, 2009.
34. **Okami T, Yamamoto A, Omori K, Takada T, Uyama M, Tashiro Y.** Immunocytochemical localization of Na^+,K^+-ATPase in rat retinal pigment epithelial cells. *J Histochem Cytochem Off J Histochem Soc* 38: 1267–1275, 1990.
35. **Palmgren MG, Nissen P.** P-type ATPases. *Annu Rev Biophys* 40: 243–266, 2011.
36. **Piermarini PM, Grogan LF, Lau K, Wang L, Beyenbach KW.** A SLC4-like anion exchanger from renal tubules of the mosquito (*Aedes aegypti*): evidence for a novel role of stellate cells in diuretic fluid secretion. *Am J Physiol Regul Integr Comp Physiol* 298: R642–R660, 2010.
37. **Puverel S, Tambutté E, Zoccola D, Domart-Coulon I, Bouchot A, Lotto S, Allemand D, Tambutté S.** Antibodies against the organic matrix in scleractinians: a new tool to study coral biomineralization. *Coral Reefs* 24: 149–156, 2005.
38. **Rizzolo LJ, Zhou S.** The distribution of Na^+,K^+-ATPase and 5A11 antigen in apical microvilli of the retinal pigment epithelium is unrelated to alpha-spectrin. *J Cell Sci* 108: 3623–3633, 1995.
39. **Roa JN, Munévar CL, Tresguerres M.** Feeding induces translocation of vacuolar proton ATPase and pendrin to the membrane of leopard shark (*Triakis semifasciata*) mitochondrion-rich gill cells. *Comp Biochem Physiol A Mol Integr Physiol* 174: 29–37, 2014.
40. **Romano SL, Palumbi SR.** Evolution of scleractinian corals inferred from molecular systematics. *Science* 271: 640–642, 1996.
41. **Romero MF, Chen AP, Parker MD, Boron WF.** The SLC4 family of bicarbonate (HCO_3^-) transporters. *Mol Aspects Med* 34: 159–182, 2013.
42. **Schmitt BM, Biemesderfer D, Romero MF, Boulpaep EL, Boron WF.** Immunolocalization of the electrogenic Na+-HCO_3^- cotransporter in mammalian and amphibian kidney. *Am J Physiol Renal Physiol* 276: F27–F38, 1999.
43. **Shinzato C, Shoguchi E, Kawashima T, Hamada M, Hisata K, Tanaka M, Fujie M, Fujiwara M, Koyanagi R, Ikuta T, Fujiyama A, Miller DJ, Satoh N.** Using the *Acropora digitifera* genome to understand coral responses to environmental change. *Nature* 476: 320–323, 2011.
44. **Silver IA, Erecińska M.** Energetic demands of the Na^+/K^+ ATPase in mammalian astrocytes. *Glia* 21: 35–45, 1997.
45. **Specht SC, Lopez-Rosado R, Santos-Berrios C, Figueroa-Nieves R.** An ouabain-sensitive Na^+,K^+-ATPase in tentacles of the sea anemone *Stichodactyla helianthus*. *Comp Biochem Physiol B Biochem Mol Biol* 110: 555–563, 1995.
46. **Stamatakis A, Hoover P, Rougemont J.** A rapid bootstrap algorithm for the RAxML Web servers. *Syst Biol* 57: 758–771, 2008.

47. **Stolarski J, Kitahara MV, Miller DJ, Cairns SD, Mazur M, Meibom A.** The ancient evolutionary origins of Scleractinia revealed by azooxanthellate corals. *BMC Evol Biol* 11: 316, 2011.
48. **Sundaram P, Echalier B, Han W, Hull D, Timmons L.** ATP-binding cassette transporters are required for efficient RNA interference in *Caenorhabditis elegans*. *Mol Biol Cell* 17: 3678–3688, 2006.
49. **Tambutté E, Allemand D, Zoccola D, Meibom A, Lotto S, Caminiti N, Tambutté S.** Observations of the tissue-skeleton interface in the scleractinian coral *Stylophora pistillata*. *Coral Reefs* 26: 517–529, 2007.
50. **Tambutté E, Tambutté S, Segonds N, Zoccola D, Venn A, Erez J, Allemand D.** Calcein labelling and electrophysiology: insights on coral tissue permeability and calcification. *Proc Biol Sci* 279: 19–27, 2012.
51. **Taylor JR, Mager EM, Grosell M.** Basolateral NBCe1 plays a rate-limiting role in transepithelial intestinal HCO_3^--secretion, contributing to marine fish osmoregulation. *J Exp Biol* 213: 459–468, 2010.
52. **Le Tissier M.** The ultrastructure of the skeleton and skeletogenic tissues of the temperate coral *Caryophyllia smithii*. *J Mar Biol Assoc UK* 70: 295–310, 1990.
53. **Tokuyasu KT.** Immunochemistry on ultrathin frozen sections. *Histochem J* 12: 381–403, 1980.
54. **Vidal-Dupiol J, Zoccola D, Tambutté E, Grunau C, Cosseau C, Smith KM, Freitag M, Dheilly NM, Allemand D, Tambutté S.** Genes related to ion-transport and energy production are upregulated in response to CO_2-driven pH decrease in corals: new insights from transcriptome analysis. *PLoS One* 8: e58652, 2013.
55. **Weis VM, Allemand D.** What determines coral health? *Science* 324: 1153–1155, 2009.
56. **Wooldridge SA.** Breakdown of the coral-algae symbiosis: towards formalising a linkage between warm-water bleaching thresholds and the growth rate of the intracellular zooxanthellae. *Biogeosciences* 10: 1647–1658, 2013.
57. **Zoccola D, Tambutté E, Kulhanek E, Puverel S, Scimeca JC, Allemand D, Tambutté S.** Molecular cloning and localization of a PMCA P-type calcium ATPase from the coral *Stylophora pistillata*. *Biochim Biophys Acta Biomembr* 1663: 117–126, 2004.
58. **Zoccola D, Tambutté E, Sénégas-Balas F, Michiels JF, Failla JP, Jaubert J, Allemand D.** Cloning of a calcium channel α_1 subunit from the reef-building coral, *Stylophora pistillata*. *Gene* 227: 157–167, 1999.